

# Effect of two vaccine doses in the SEIR epidemic model using a stochastic cellular automaton

Enrique C. Gabrick<sup>1a</sup>, Paulo R. Protachevicz<sup>2</sup>, Antonio M. Batista<sup>1,3</sup>, Kelly C. Iarosz<sup>4,5</sup>, Silvio L. T. de Souza<sup>6</sup>, Alexandre C. L. Almeida<sup>7</sup>, José D. Szezech Jr<sup>1,3</sup>, Michele Mugnaine<sup>8</sup>, Iberê L. Caldas<sup>2</sup>

<sup>1</sup>Postgraduate Program in Sciences, State University of Ponta Grossa, 84030-900, Ponta Grossa, PR, Brazil

<sup>2</sup>Physics Institute, University of São Paulo, 05508-090, São Paulo, SP, Brazil

<sup>3</sup>Department of Mathematics and Statistics, State University of Ponta Grossa, 84030-900, Ponta Grossa, PR, Brazil

<sup>4</sup>Faculdade de Telêmaco Borba, FATEB, Telêmaco Borba, PR, Brazil

<sup>5</sup>Graduate Program in Chemical Engineering Federal Technological University of Paraná, Ponta Grossa, PR, Brazil

<sup>6</sup>Federal University of São João del-Rei, Campus Centro-Oeste, 35501-296, Divinópolis, MG, Brazil

<sup>7</sup>Statistics, Physics and Mathematics Department,

Federal University of São João del-Rei, Ouro Branco, MG, Brazil and

<sup>8</sup>Department of Physics, Federal University of Paraná, Curitiba, PR, Brazil

In this work, to support decision making of immunisation strategies, we propose the inclusion of two vaccination doses in the SEIR model considering a stochastic cellular automaton. We analyse three different scenarios of vaccination: (i) unlimited doses, (ii) limited doses into susceptible individuals, and (iii) limited doses randomly distributed overall individuals. Our results suggest that the number of vaccinations and time to start the vaccination is more relevant than the vaccine efficacy, delay between the first and second doses, and delay between vaccinated groups. The scenario (i) shows that the solution can converge early to a disease-free equilibrium for a fraction of individuals vaccinated with the first dose. In the scenario (ii), few two vaccination doses divided into a small number of applications reduce the number of infected people more than into many applications. In addition, there is a low waste of doses for the first application and an increase of the waste in the second dose. The scenario (iii) presents an increase in the waste of doses from the first to second applications more than the scenario (ii). In the scenario (iii), the total of wasted doses increases linearly with the number of applications. Furthermore, the number of effective doses in the application of consecutive groups decays exponentially overtime.

*Keywords:* SEIR, COVID-2019, Vaccine, Cellular automata, Stochastic model, Spread disease.

## I. INTRODUCTION

Understanding the dynamics of epidemics is an important interdisciplinary research topic [1]. The studies can provide contribution to the prevention and control of infectious diseases [2]. An epidemic is the fast spread of infectious diseases that produce many infected individuals within a population [3]. Some examples of epidemics are the bubonic plague or Black Death during the fourteenth century [4], Spanish flu in 1918 [5], Severe Acute Respiratory Syndrome (SARS) in 2002 [6], H1N1 in 2009 [7], and, more recently, in the end of 2019, the novel coronavirus (COVID-19) arose in Hubei Province in China [8].

There are many ways that can be used to control the infectious disease spread, for instance the minimisation of the social contact [9], quarantine [10], restrictions [1], lockdown [11], and others [2]. One of the most effective strategies is the application of vaccines [12]. Most mathematical models consider only one dose [10, 12]. For some diseases, there are vaccines that are administered in two doses, for instance, for the novel coronavirus [12]. With this in mind, we include two new compartments in the SEIR model to simulate two doses of vaccination. Our SEIR model is described by a stochastic cellular automaton and can be adapted for many diseases.

Mathematical models have been used to analyse the dynamical behaviour of epidemics and evaluate strategies to control them [13–15]. In general, the population is separated into compartments in the mathematical models of infectious diseases, such as SIS, SIR, SEIR, and SEIRS [16]. The compartments can be susceptible ( $S$ ), exposed ( $E$ ), infected ( $I$ ), and recovered ( $R$ ) individuals. In this work, we choose the SEIR model [17], which can be studied from differential equations [17] or cellular automata approach. Nevertheless, our model can be modified for the SIR model.

In the SEIR model, the host population is divided into four compartments [18]:  $S$  (susceptible) represents the individuals who can be infected, when in contact with infected individuals,  $E$  (exposed) are the individuals in latent [11, 16] and/or incubation period [15, 19]. The latent period corresponds to the range time in which the individuals do not transmit the disease [16]. On the other hand, during the incubation period, the exposed individuals can transmit the disease with a lower incidence than infected individuals [15]. In our simulations,  $E$  corresponds to a latent period.  $I$  (infected) is associated with the individuals that are infected and can transmit the disease.  $R$  (recovered) is related

---

<sup>a</sup> ecgabrick@gmail.com

to the individuals that get immunity or die. The scenario studied does not consider the possibility of reinfection. This model was considered to simulate the impact of easing restrictions [1], scenarios with reinfection [20], inclusion of vaccine [21], spatiotemporal evolution of epidemics [2]. More recently, Sharma et al. [11] considered a SEIRD model (Death) with delay to predict the evolution of pandemic in India. They analysed scenarios with no lockdown, strict lockdown, and movement with social distancing.

Etzeberria-Etxaniz et al. [22] considered the vaccination of newborns and periodic impulse vaccination in the SEIR model. A stochastic formulation of the SEIR model with the inclusion of vaccination was studied by Balsa et al. [10]. They considered the combination of vaccination and quarantine. Jadidi et al. [23] proposed the vaccination in two steps, vaccine allocation, and targeted vaccination. The SEIR model with quarantine, isolation, and imperfect vaccine was analysed by Safi and Gumel [24]. Yongzhen et al. [25] reported the effect of constant and pulse vaccination on the SIR model with an infectious period. In the SIR model, White et al. [3] included vaccine using cellular automata. Nava et al. [26] studied how controllable parameters can lower the infection spread in an open crowded space. They considered the generalised SEIR model with an analytical and cellular automaton approach.

Most of the works considered one dose of vaccine. Recently, De la Sen et al. [27] proposed a SEIR discrete model with two vaccination doses that are applied in susceptible individuals. They discussed the influence of the vaccination starting time, as well as the effect of the delay between the first and second doses.

In this work, we propose an epidemic SEIR model with two doses vaccinations based on stochastic cellular automata (CA) [28–30]. In the deterministic context, Wolfram defined the CA as discrete idealisations [31, 32]. Deterministic CA evolves in accordance with deterministic transition rules [29, 33], while the stochastic evolves in accordance with stochastic transition rules [34]. Furthermore, the transition rules can be a mix of deterministic and probabilistic ones [35, 36]. One advantage of the CA is the possibility of including local features in the model [37]. CA have been applied in various areas, for instance physics [38] and biology [39, 40]. Santos et al. [41] reported that a CA model can reproduce time series of dengue epidemics. Recently, Blavatska and Holovatch [42] investigated infection spreading processes in a CA where only a fraction of individuals is affected by a disease. Mikler et al. [43] studied a stochastic CA to simulate a SIR model with geographic and demographic characteristics, as well as migratory constraints. In addition, Cavalcante et al. studied a SEIR model by means of differential equations and CA [44].

We consider three scenarios of vaccination: *(i)* unlimited doses in susceptible individuals by means of continuous vaccination, *(ii)* limited doses in susceptible individuals through pulse periodic vaccination, and *(iii)* limited doses that are randomly distributed. In the scenario *(i)*, we obtain the variation of the infected individual numbers as a function of the time of starting the application, the delay between the first and second doses, and the vaccine efficacy influence. The scenario *(ii)* permits to find effective ways to manage few doses. In the scenarios *(ii)* and *(iii)*, individuals are vaccinated and the effect occurs only in the susceptible individuals. For these scenarios, we estimate the occurrence of wasted doses, applied to individuals who received the first dose and are infected before the second dose, as a function of the considered control parameters. We show that the waste in the first dose occurs when the available doses are bigger than the number of susceptible individuals or the first dose is applied in the individuals outside the susceptible state (third scenario). Furthermore, we show that the number of vaccinations and time to start the vaccination is more relevant than the vaccine efficacy, delay between first and second dose, and delay between vaccinated groups. In the scenario *(ii)*, few two vaccination doses divided into a small number of applications reduce the quantity of infected people more than into many applications. In addition, there is a low waste of doses for the first application and an increase of the waste in the second dose. The scenario *(iii)* presents an increase in the waste of doses from the first to second applications more than the scenario *(ii)*. In the scenario *(iii)*, the total of wasted doses increases linearly with the number of applications. The number of effective doses in the application of consecutive groups decays exponentially overtime.

The paper is organised as follows. In Section 2 the model is presented in details. In Section 3, numerical simulations of the scenario *(i)* are discussed. Section 4 shows numerical simulations of the scenerii *(ii)* and *(iii)*. Finally, Section 5 presents our conclusions.

## II. DESCRIPTION OF THE MODEL

Cellular automata are mathematical models characterised by discrete time, space, and state variables. In our model, each time step is taken to be one day. The transitions between states occur by local rules. In this work, we build a two-dimensional CA with deterministic and probabilistic transition rules. The CA is given by a lattice ( $L$ ) composed of  $N \times N$  identical cells [45] with

$$L = (i, j), \quad i, j \in Z_+^* \mid 1 \leq i, j \leq N. \quad (1)$$

Each cell is identified by one state  $x(i, j, t) \in U$ , where the set  $U = \{1, 2, 3, 4\}$  indicates the  $\{S, E, I, R\}$  states, respectively. For each cell  $(i, j)$ , a Moore's neighbourhood  $V$  is considered and given by  $M(i, j) = (i, j) + v$ , where

$v \in V$  and  $V$  is defined as

$$V = \{(0, 0), (-1, 0), (-1, -1), (-1, 1), (1, 0), (1, -1), (1, 1), (0, -1), (0, 1)\}. \quad (2)$$

The boundary conditions represented by  $(i, j) \notin L$  [3] are given by  $x(i, j, t) = 0$ . With this boundary condition the cells are disposed in a plan. The cells inside of the region delimited by  $N \times N$  do not interact with the boundary cells. One time step (one day) is defined when all cells in the lattice are updated in accordance with transition rules.

We consider parameters based on various sources in the literature. The values of the transmission rate are obtained from Balsa et al. [10]. From Radulescu [17], we use the values related to the infectious period, time to develop symptoms, and infection rate. The time between doses is obtained from De la Sen et al. [27] and the vaccine efficacy from Voysey et al. [8].

### A. Transmission model without vaccination

The total population  $N \times N$  is separated into four compartments, as shown in Fig. 1. The susceptible, exposed, infected, and recovered cells are represented by  $S(t)$ ,  $E(t)$ ,  $I(t)$ , and  $R(t)$ , respectively. Individuals in the compartmental  $S$  can become  $E$  with probability  $\beta$  when there are  $I$  neighbours. After  $\tau_1$  times, there is a rate  $\lambda$  in which individuals go from  $E$  to  $I$ . They stay during  $\tau_2$  time step in  $I$  (infectious period) and then go to  $R$ . In the model, we consider that recovered cells have a permanent immunity. The initial condition is given by a random distribution of infected cells  $I(0)$ . The major part of the cells is initially in the susceptible state. The exposed and recovered cells are not considered in the initial time of the simulation.

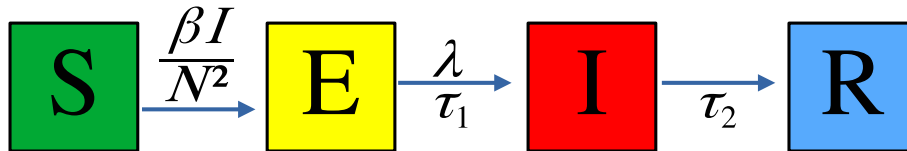


FIG. 1. Schematic representation of the SEIR model.  $\beta$  is the probability of the susceptible individuals become exposed and  $\lambda$  is the rate of exposed individuals become infected.  $\tau_1$  and  $\tau_2$  correspond to the time intervals in which exposed and infected individuals remain in the same state, respectively.

The update rule of the individual  $(i, j)$  in absence of vaccination depends on its initial state and their neighbouring states in the previous time, as well as on the transition probability  $\beta$  and  $\lambda$  from the exposed to infected states, and the time constants  $\tau_1$  and  $\tau_2$ . The evolution of the CA can be expressed by a time function  $F$  given by

$$F(i, j, t) = f(x(i, j, t-1), \dots, x(i, j, t-\tau), x(i+\alpha, j+\gamma, t-1), \beta, \lambda), \quad (3)$$

where  $(\alpha, \gamma) \in V$ ,  $\tau \in (\tau_1, \tau_2)$ .

The transition rules can be summarised as:

- Each infected cell ( $x(i, j, t) = 3$ ) can infect a neighbour in a susceptible state ( $x(i, j, t) = 1$ ) with probability  $\beta$ . In other words, if the cell is in the susceptible state with one or more (up to eight) infected neighbours, each infected cell will try to transmit the disease to the susceptible with a probability  $\beta$ . Once infected, the susceptible cell ( $x(i, j, t) = 1$ ) will evolve in the next step (day) to the exposed state ( $x(i, j, t) = 2$ ).
- After evolving to the exposed state ( $x(i, j, t) = 2$ ), the cells stay in this state by  $\tau_1$  time steps (days units). In the next step, a fraction  $\lambda$  of exposed cells evolve to the infected state ( $x(i, j, t) = 3$ ).
- If the cells are infected ( $x(i, j, t) = 3$ ), they remain in the infected state by  $\tau_2$  time steps. After  $\tau_2$ , infected cells evolve to a recovered state ( $x(i, j, t) = 4$ ).
- After evolving to the recovered state ( $x(i, j, t) = 4$ ), the cells stay in there all the time.

An illustration of one spatial time evolution of the CA is displayed in Fig. 2. In Fig. 2(a), we see the states distribution for  $t = 300$ . Figure 2(b) exhibits the magnification of the region delimited in the panel (a) by a white square. Figures 2(c) and 2(d) show the spatial evolution for  $t = 600$  and  $t = 900$ , respectively. In Fig. 2(b), the borders composed of green and red cells represent the individuals in the exposed and infected states, respectively. These borders evolve overtime in circular waves from the central region, as shown by means of the blue cells that represent the recovered states. In the final evolution of the system, the lattice exhibits only blue cells, which is the disease-free equilibrium solution, where the eradicating of the illness is found.

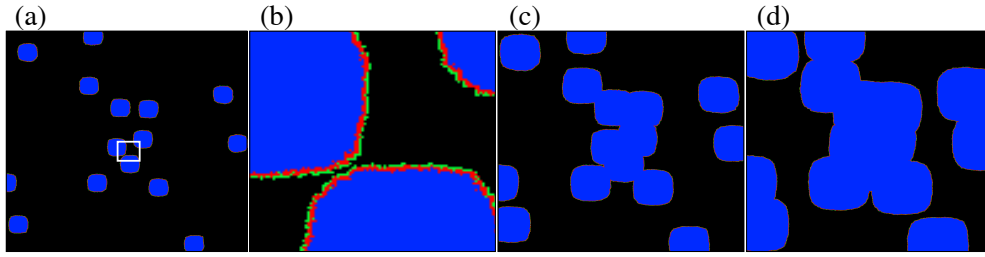


FIG. 2. Spatial time evolution of the CA for  $N = 1000$ ,  $I(0) = 15$ ,  $\lambda = 1/3$ ,  $\beta = 1/4$ ,  $\tau_1 = 6$ ,  $\tau_2 = 14$ . (a) States distribution for  $t = 300$  and (b) magnification of the region delimited by the white square in panel (a). The panels (c) and (d) show the states distribution for  $t = 600$  and  $t = 900$ , respectively. In the black, red, green, and blue regions, we observe the susceptible, infected, exposed, recovered states, respectively.

### B. Transmission model with vaccination

In our CA model, we include vaccinations that are divided into unlimited and limited doses. In this case, we consider the states  $U = \{1, 2, 3, 4, 5, 6\}$ , where the two new ones  $x(i, j, t) = 5$  and  $x(i, j, t) = 6$  represent the cells that receive the first  $V_1$  and second  $V_2$  doses of the vaccine. Figure 3 displays the schematic representation of the SEIR model with the first and second doses, named as SEIR2V. This schematic representation is valid for the scenario (i) (unlimited doses) and scenario (ii) (limited doses), where only the susceptible cells are vaccinated. In the scenario (iii), the vaccine doses are randomly distributed in all lattice.

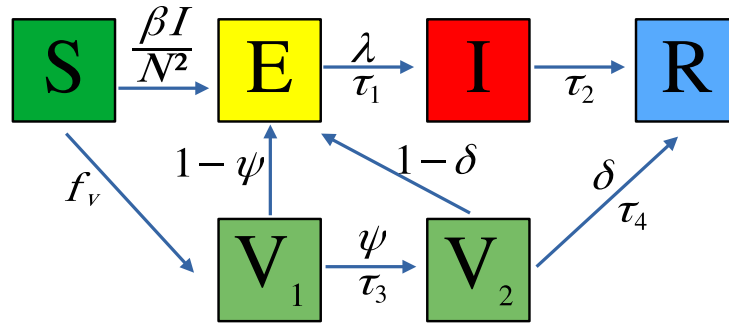


FIG. 3. SEIR model with two vaccination doses. The first and second doses are the two new cell states, being represented by  $V_1$  and  $V_2$ . The parameters  $f_v$  define the fraction of the susceptible that receive the first dose.  $\psi$  and  $\delta$  correspond to the first and second doses efficacy, respectively.  $\tau_3$  is the time interval between the first and second doses, and  $\tau_4$  is the time to arrive in the recovered state from the  $V_2$ .

The scenarios for vaccine application are illustrated in Fig. 4. The blue bars indicate the total available first doses and the green bars correspond to the second doses. First, we consider the scenario (i), as illustrated in Fig. 4(a). In the time  $t_{v_1}$ , a fraction  $f_v$  of susceptible cells are vaccinated with the first dose, evolving to the  $V_1$  state. In the time  $t_{v_1} + 1$ , another susceptible fraction ( $f_v$ ) receives the first dose. And so on, every day, until the infected number goes to zero. In this sense, we say that available doses are unlimited. The cells that go to the first dose vaccinated state  $V_1$ , remain in this state during  $\tau_3$  time steps before receiving the second dose. The time  $\tau_3$  is the delay between the first and second doses. The probability of these cells get infected is  $1 - \psi$ , where  $\psi$  is the first dose efficacy. After  $\tau_3$  (time delay), in  $t_{v_2}$ , the second dose is applied in the cells in  $V_1$  states. The cells, that get the second dose, are the cells that were not infected while stay in  $V_1$  state. After receiving the second dose, the probability of the cells in  $V_2$  states get infected is  $1 - \delta$ , where  $\delta$  is the booster efficacy. The cells, that are not infected in the period  $\tau_4$ , evolve to  $R$  state. Fig. 4(b) illustrates the (ii) scenario, where the amount of dose is a fixed number, given by  $D_T = f_v \cdot N^2$ . The vaccination starts at  $t_{v_1}$  with the application of  $D_T$  doses in the susceptible cells. The next group receives the first dose after  $\Delta t_v$  times in a pulsed way. The application of the second dose occurs in the same way. The second dose application starts in  $t_{v_2}$  with  $D_T$  doses that will be applied in uninfected cells belonging to the first vaccinated group. The different susceptible groups and  $V_1$  groups, that receive the first and second doses, are denoted by  $m$  with  $m \in Z_+^*$ . The time application of the first and second doses in subsequently cell groups is given by  $t_{v_{1,2}}^m = t_{v_{1,2}}^{m-1} + \Delta t_v$ ,

where  $m \geq 2$ ,  $t_{v_{1,2}}^1 = t_{v_{1,2}}$ , and  $\Delta t_v$  is the interval between the applications. In this context, the (i) scenario has  $\Delta t_v = 1$ . Fig. 4(c) illustrates the (iii) scenario. The application protocols are the same that (ii) scenario. The difference is that instead of applying the first dose in susceptible cells, the application of  $D_T$  doses occurs in all cells that belong to the lattice. However, the effect occurs only in susceptible cells. In this sense, we use the term wasted doses to refer to the doses given to exposed, infected, or recovered individuals. These applied doses will not contribute to preventing newly infected individuals. In this way, the total number of doses is represented by  $N_T = D_T \cdot N_{App}$ , where  $N_{App}$  is the total number of applications. The total amount of vaccines in each dose  $D_T$  can be identified as the sum of the effective ( $D_{eff}$ ) and wasted doses ( $D_w$ ), corresponding to  $D_T = D_{eff} + D_w$ .

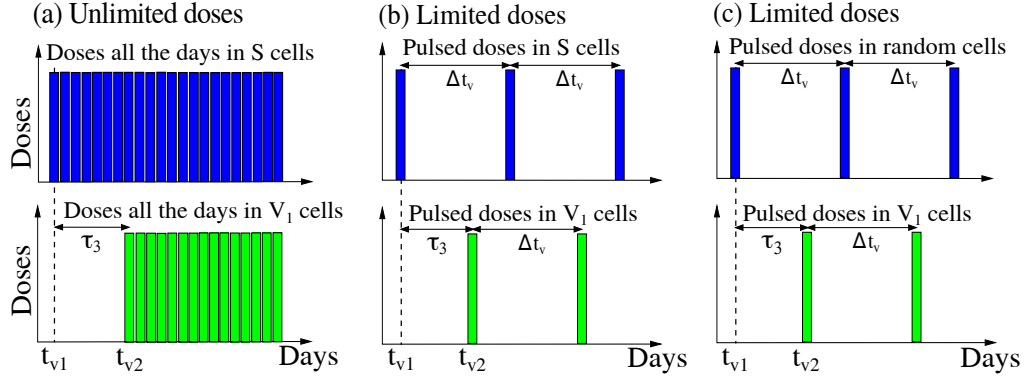


FIG. 4. Schematic representation of three scenarios for vaccination. The panel (a) illustrates the (i) scenario. The panel (b) is a schematic representation of the (ii) scenario, and the panel (c) is the representation of the (iii) scenario. The blue bars indicate the amount for first dose and the green bar correspond to the second dose.

To simulate the CA with the two new compartments, we consider new rules:

- Given a cell in  $V_1$  state, if this cell has one or more infected neighbours, it can be infected with  $1 - \psi$  probability, where  $\psi$  is the first dose efficacy. If the vaccinated cell is infected, it evolves to an exposed state, such as a susceptible cell in the model without vaccination.
- The uninfected cells in  $V_1$ , evolve to  $V_2$  state after a time delay,  $\tau_3$ .
- If the cell in  $V_2$  has one or more neighbours in an infected state, it can be infected with  $1 - \delta$  probability, where  $\delta$  is the booster efficacy. If the vaccinated cell is infected, it evolves to an exposed state. The cells that cannot be infected evolve to the recovered states after  $\tau_4$ .

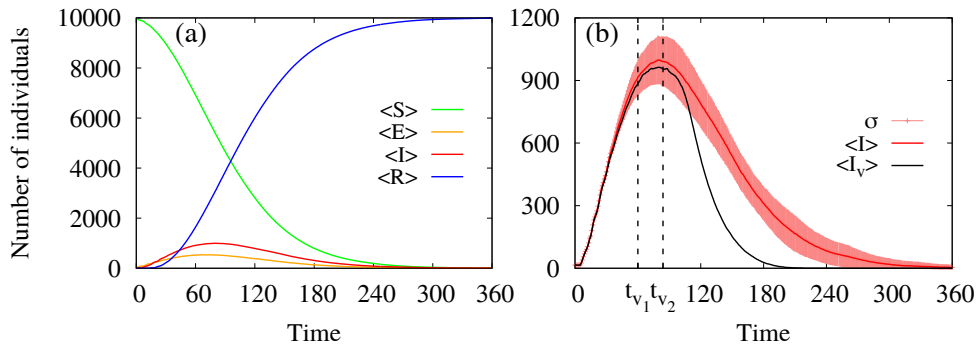


FIG. 5. (a) Average time of the SEIR model without vaccination. The green, orange, red, and blue lines denote  $\langle S \rangle$ ,  $\langle E \rangle$ ,  $\langle I \rangle$ , and  $\langle R \rangle$ , respectively. (b) Number of infected individuals for the case without vaccination (red line), where  $\sigma$  is the standard deviation for 50 simulations, and for the scenario (i) with vaccination (black line). We consider  $\beta = 1/4$ ,  $\lambda = 1/3$ ,  $\tau_1 = 6$ ,  $\tau_2 = 14$ . In the panel (b), the parameters of the vaccination are  $t_{v_1} = 60$ ,  $t_{v_2} = 84$  (indicated by vertical dashed lines),  $\tau_3 = 24$ ,  $\tau_4 = 10$ ,  $f_v = 0.02$ ,  $\psi = 0.66$ , and  $\delta = 0.75$ . The time unit is day.

Figure 5(a) shows the time evolution of the SEIR model without vaccine application, where the green, orange, red, and blue lines represent the average of susceptible, exposed, infected, and recovered cells, respectively. In Fig.

5(b), we present the infected curve for the scenario (i) of vaccination (black line) and no vaccine (red line). In the considered example, the first and second vaccination times are, respectively,  $t_{v_1} = 60$  and  $t_{v_2} = 84$ . With and without vaccination control, the disease eradication is obtained for  $T_0 = 218$  and 360 time steps, respectively.

In Sections 3 and 4, we consider  $N = 100$ ,  $\lambda = 1/3$ ,  $\beta = 1/4$ ,  $\tau_1 = 6$  days,  $\tau_2 = 14$  days,  $\tau_3 = 24$  days,  $\tau_4 = 10$  days. The initial numbers of cells are given by  $I(0) = 15$ ,  $S(0) = N^2 - I(0)$ , and  $E(0) = R(0) = V_1(0) = V_2(0) = 0$ . Our results are calculated by means of an average of 50 independent repetitions, denoted by  $\langle \cdot \rangle$ .

### III. UNLIMITED DOSES

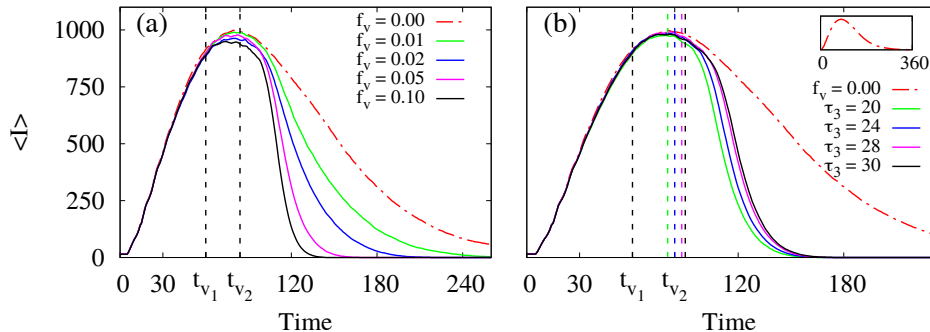


FIG. 6. (a) Average of infected cells overtime for different values of  $f_v$ . Vertical black dashed lines indicate the starting of the first ( $t_{v_1} = 60$ ) and second ( $t_{v_2} = 84$ ) doses. In the panel (b), infected cells overtime for different values of  $\tau_3$  and  $f_v = 0.05$ . The vertical coloured lines represent the starting of the second dose vaccination for different values of  $\tau_3$ . The red dash-dotted line represents the case without vaccination. In the panel (b), the insert shows the whole curve. The considered value of vaccination efficacy for the first and second doses are  $\psi = 0.66$  and  $\delta = 0.75$ . The time unit is day.

Figures 6(a) and 6(b) exhibit the infected cells overtime due to the influence of different values of  $f_v$  and  $\tau_3$ , respectively. The red dash-dotted line represents the case without vaccination. The vertical black dashed line indicates the start of the first and second doses. In Fig. 6(a), the infected curve suffers narrowing when  $f_v$  is increased, implying in the decrease of the area under the respective curve. The normalised area ( $A_n = 1$ ) covers the red dash-dotted curve. Increasing the  $f_v$  values from zero, the normalised areas are equal to  $A_n = 0.80, 0.70, 0.62$ , and  $0.57$ , respectively. As a result, the system goes to the disease-free equilibrium point earlier. In Fig. 6(b), we observe that an increase in  $\tau_3$  generates wider infected curves. The green, blue, magenta, and vertical black dashed lines indicate the start time of the second dose considering  $\tau_3 = 20, 24, 28$ , and  $30$ , corresponding to  $A_n = 0.59, 0.62, 0.65$ , and  $0.65$ , respectively. For  $\tau_3 \geq 20$  occurs an increase in the area, however, the influence of this parameter on the dynamics is less pronounced than  $f_v$ .

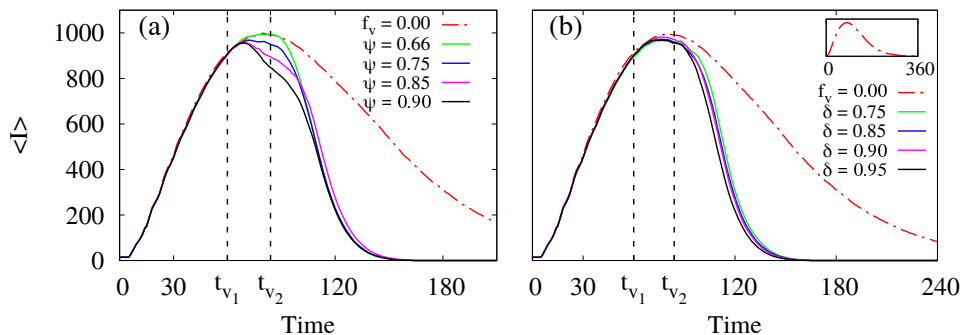


FIG. 7. (a) Average of infected cells overtime for different values of  $\psi$  for  $\delta = 0.95$  and  $f_v = 0.05$ . (b) Different values of  $\delta$  overtime for  $\psi = 0.66$  and  $f_v = 0.05$ . The vertical dashed lines indicate the time in which the first and second doses are administrated. The red dash-dotted line corresponds to the case without vaccination. The time unit is day.

We investigate the influence of the efficacy of the first and second doses, denoted by  $\psi$  and  $\delta$ , respectively, in the infected curves. Figures 7(a) and 7(b) display the infected curves overtime for different values of  $\psi$  and  $\delta$ . In Fig.



7(a), we see that the infected curve goes faster to zero for large values of  $\psi$ . In this case, we consider the second dose efficacy as  $\delta = 0.95$ . For  $\psi = 0.66$ , Figure 7(b) shows that the infected curve is narrowed when  $\delta$  is increased. In both cases, the areas do not change significantly. Therefore, for this range of values, we do not observe significant effect on the dynamical system.

Figure 8(a) exhibits the time for disease eradicating ( $T_0$ ) as a function of  $t_{v_1}$  and  $f_v$ . In Fig. 8(b), we calculate the normalised area ( $A_n$ ) under the infected curve as a function of  $t_{v_1}$  and  $f_v$ . Our results show that earlier to start the first dose application more effective is the vaccine. The  $f_v$  values larger than 0.01 affect positively the dynamics for  $t_{v_1} \leq 30$ , namely, for these values  $T_0$  and  $A_n$  are significantly reduced. For small  $f_v$  or large  $t_{v_1}$  values, the effect of vaccination on  $T_0$  can occur, however, it is reduced. The major reduction in  $T_0$  and  $A_n$  happens for large  $f_v$  and small  $t_{v_1}$ . For  $f_v \leq 0.01$ , the effects of  $T_0$  are smaller than  $f_v \approx 0.01$ . The total number of infected individuals is smaller for  $f_v \geq 0.01$ , as shown in Fig. 8(b).

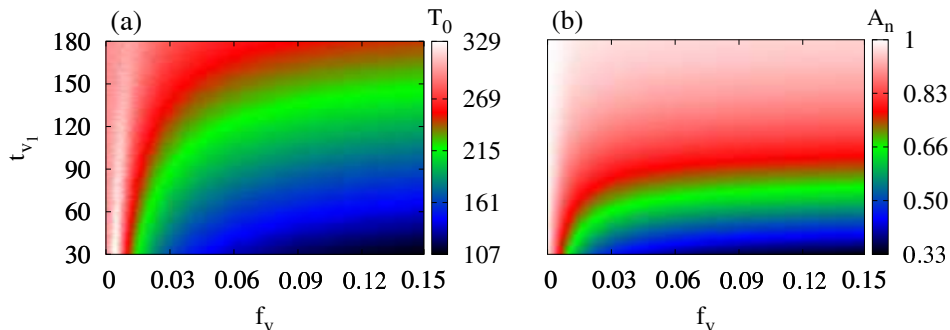


FIG. 8. (a) Time for the disease eradicating ( $T_0$ ) and (b) normalised area under the infected curve ( $A_n$ ) as a function of  $t_{v_1}$  and  $f_v$  for  $\psi = 0.66$  and  $\delta = 0.75$ . The time unit is day.

#### IV. LIMITED DOSES

In the scenario (ii), we investigate the effect of different times among different groups who received the first and second doses ( $\Delta t_v$ ) in the susceptible cells. We consider  $f_v = 0.03$  and  $D_T = 300$  for each application, as well as we vary the values of  $\Delta t_v$ , as shown in Fig. 9(a). The values of  $A_n$  are equal to 0.58, 0.73, 0.79, and 0.89 for the green, blue, magenta and black curves, respectively. Then, an increase in  $\Delta t_v$  contributes to an increase in  $A_n$ . Therefore, the vaccine is more effective for small values of  $\Delta t_v$ .

Figure 9(b) shows the influence of  $f_v$  for  $\Delta t_v = 7$ . In the scenario (ii), the wasted doses in the first dose vaccination occur when  $D_T$  is larger than the number of susceptible individuals. For  $f_v = 0.01$  (green curve),  $f_v = 0.03$  (blue curve),  $f_v = 0.06$  (magenta curve), and  $f_v = 0.15$  (black curve) the cells number who receive the first dose are  $D_{\text{eff}} \approx 1500, 3621, 4835, \text{ and } 6073$ , respectively. The  $A_n$  values are given by 0.92, 0.78, 0.70, and 0.60. For  $f_v = 0.01$ , the number of infected individuals goes to zero approximately when there is no vaccination. For large values of  $f_v$ , the number of infected individuals goes to zero faster. The increase of  $f_v$  implies in a reduction of the area and the equilibrium point is achieved earlier.

Figure 10 displays the effect of dividing the total amount of doses  $N_T$  into many applications  $N_{\text{App}}$  that are spaced out by  $\Delta t_v = 7$  with  $N_{\text{App}} \in Z^*$ . Figures 10(a) and 10(b) exhibit the dynamics for  $N_T = 3621$  and the time distribution of first and second vaccine doses for  $N_{\text{App}} = 12$ . The values of  $A_n$  are equal to 0.74, 0.77, and 0.79. Figure 10(c) shows the time series for  $N_T = 6073$  and the time distribution of vaccine for  $N_{\text{App}} = 12$  is shown in 10(d). In Figs. 10(b) and 10(d), the blue and green bars indicate the effective doses in the first and second doses applications, respectively. The gray bars denote the total quantity of available first doses ( $D_T$ ). For simplicity, the total quantity of available second doses is omitted in the figures, however, the same  $D_T$  is displaced in time. The effectiveness of the first doses, represented by the blue bars, is equal to  $D_{\text{eff}} = 3503$  in the panel (b) and  $D_{\text{eff}} = 4529$  in the panel (d). In the last applications of the first doses, we observe a decrease in the effective doses. This behaviour occurs due to the number of available dose ( $D_T$ ) to be larger than the number of susceptible cells. The effectiveness of the second dose, represented by the green bars, suffers a higher decrease in the amplitude, that occurs by a sum of factors. The cells that receive the second doses come from the successful first doses. In this way, it is expected a wasted of at least  $1 - \psi$  in the  $V_2$  state for the range time that  $D_T$  is not larger than the number of susceptible individuals. This behaviour can be seen in the time distribution shown in Fig. 10(b).

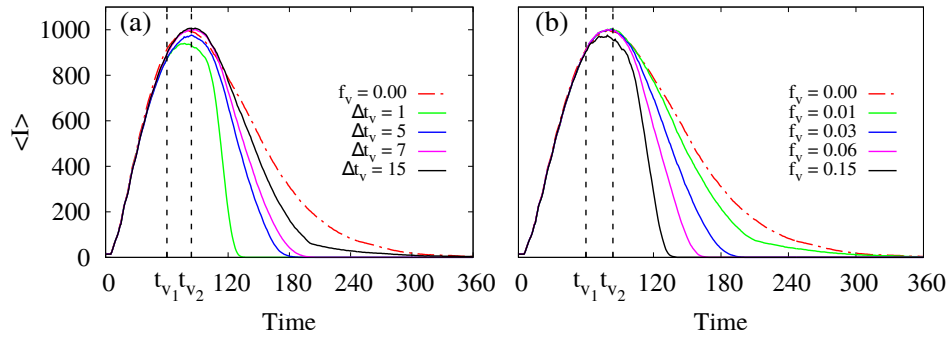


FIG. 9. (a) Average of infected cells overtime for different values of  $\Delta t_v$  and  $f_v = 0.03$ . The green, blue, magenta, and black lines correspond to the values of  $\Delta t_v$  equal to 1, 5, 7, and 15, respectively. (b) Average of infected cells overtime for different values of  $f_v$  and  $\Delta t_v = 7$ . The green, blue, magenta, and black curves correspond to the values of  $f_v$  equal to 0.01, 0.03, 0.06, and 0.15, respectively. The vertical dotted lines indicate the first and second doses applied in the first cell groups. The red dash-dotted line represents the situation without vaccination. The parameters for vaccination are given by  $\psi = 0.66$ ,  $\delta = 0.75$ ,  $t_{v_1} = 60$ , and  $t_{v_2} = 84$ . The time unit is day.

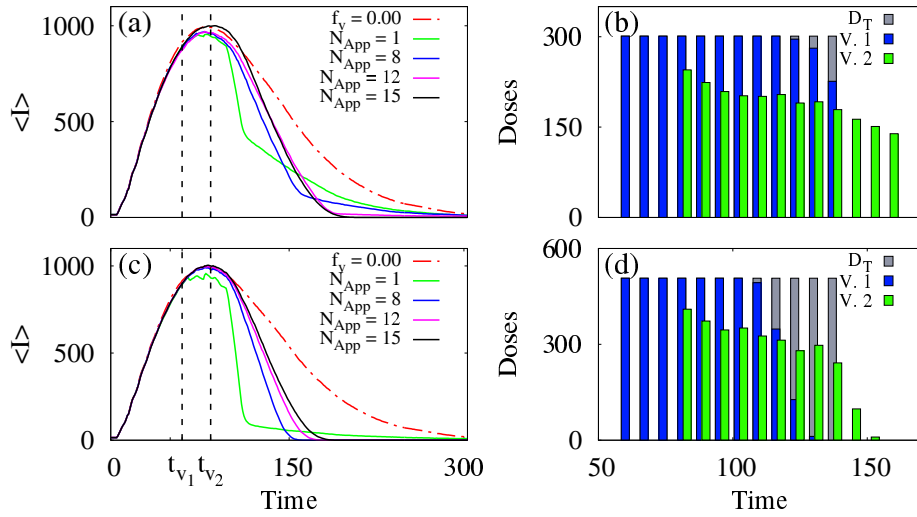


FIG. 10. (a) Average of infected curve overtime for different values of  $N_{App}$  and  $N_T = 3621$  for each dose. (b) Time distribution of first and second vaccine doses for  $N_{App} = 12$  in the panel (a). (c) Average of infected curve overtime for different values of  $N_{App}$  and  $N_T = 6073$  for each dose. (d) Time distribution of vaccine doses for  $N_{App} = 12$  in the panel (c). In the infected curves, the green, blue, magenta, and black lines correspond to  $N_{App} = 1, 8, 12,$  and  $15$ , respectively. The vertical black dashed lines indicate the time of the first and second doses for the first cell groups. The red dash-dotted line represents the case without vaccination. In the time distribution of vaccines, the blue and green bars represent the first and second effective doses, respectively. We consider  $\psi = 0.66$ ,  $\delta = 0.75$ ,  $t_{v_1} = 60$ ,  $t_{v_2} = 84$ , and  $\Delta t_v = 7$ . The time unit is days.

In Fig. 10(c), the behaviour significantly depends on  $N_{App}$ . The  $A_n$  values are 0.58, 0.68, 0.73, and 0.75. Therefore, the same doses quantity has an effect more pronounced for a small number of applications, despite the eradication point is reached later. In Fig. 10(d), the blue bars decrease due to the fact that the number of susceptible individuals is less than the available doses. In the green bars, the decrease occurs by the same effect that in Fig. 10(b). The decay is more pronounced by the decrease in the blue bar.

The scenario (iii) is similar to the scenario (ii), except that the doses are randomly distributed over all cells. Figure 11(a) shows the infected cells overtime for some values of  $f_v$  for  $\Delta t_v = 7$ . Figure 11(b) displays the time distribution of the available vaccine  $D_T$  (gray bar), and the effective first (blue bar) and second (green bar) doses for  $f_v = 0.03$ . In Fig. 11(a), the normalised area under the green, blue, magenta, and black curves are  $A_n = 0.91, 0.83, 0.69,$  and  $0.59$ , respectively. Similar results are found in the scenario (ii) (Fig. 9(b)), namely, the vaccination becomes more effective for large  $f_v$ . However, the wasted doses in  $V_1$  and  $V_2$  are larger. This occurs due to the fact that the cells leave the susceptible state overtime.



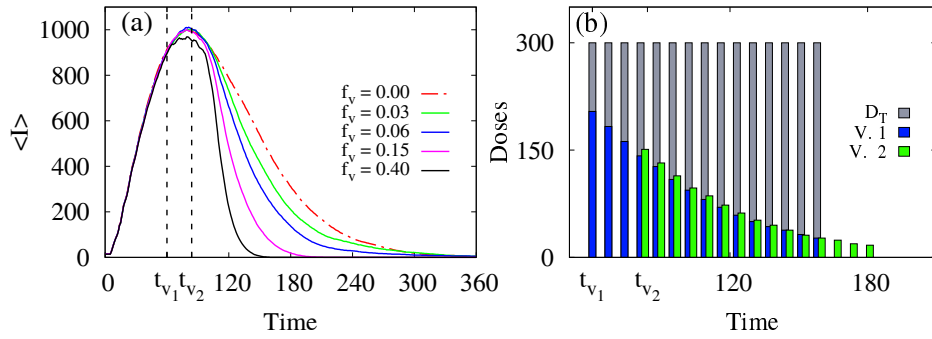


FIG. 11. (a) Average infected curve overtime for different values of  $f_v$ . The green, blue, magenta, and black curves denote the results for  $f_v$  equal to 0.03, 0.06, 0.15, and 0.40. The vertical dashed lines indicate the starting of vaccination. The red dash-dotted line is without vaccination. (b) Time distribution of the effective doses for  $f_v = 0.03$ . The gray bar indicates the available quantity of each dose ( $D_T$ ), the blue bar indicates the effective first dose ( $V_1$ ), and the green bar denotes the effective second dose ( $V_2$ ). We consider  $\psi = 0.66$ ,  $\delta = 0.75$ , and  $\Delta t_v = 7$ . The time unit is day.

The influence of  $\Delta t_v$  on the infected curves is shown in Fig. 12(a) for  $f_v = 0.03$ . The values of  $A_n$  are equal to 0.65, 0.88, 0.91, and 0.95 for the green, blue, magenta, and black curves, respectively. In Fig. 12(b), the time vaccine distribution shows the effective doses for the first  $V_1$  (blue bars) and second  $V_2$  (green bars) applications, as well as the available doses  $D_T$  (gray bars). The fraction of wasted doses is 0.68 for  $V_1$  and 0.78 for  $V_2$ . We verify that the vaccine intervention is more effective for smaller  $\Delta t_v$ , however, the wasted doses are larger.

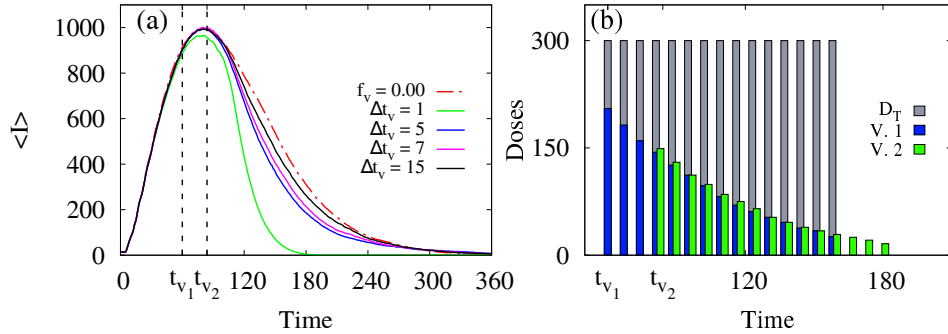


FIG. 12. (a) Infected cells curves in the scenario (iii) considering different values of  $\Delta t_v$ . The green, blue, magenta, and black curves correspond to  $\Delta t_v = 1, 5, 7,$  and  $15$ , respectively. The vertical black dashed lines indicate the time of application of the first and second doses at  $t_{v_1} = 60$  and  $t_{v_2} = 84$ . The red dash-dotted line corresponds to the case without vaccination. (b) Time distribution of the vaccine, where the gray bar is the total dose available ( $D_T$ ), the blue bars correspond to the effective dose for the first dose ( $V_1$ ), and the green bar is the effective dose for the second dose ( $V_2$ ). We consider  $\psi = 0.66$ ,  $\delta = 0.75$ ,  $f_v = 0.03$ . The time unit is day.

We investigate the influence of the number of applications considering the scenario (iii). The results in Fig. 13 are similar to Fig. 10 (scenario (ii)). Figure 13(a) shows the time evolution of the infected curve for 3621 doses and  $N_{App}$  equal to 1 (green), 8 (blue), 12 (magenta), and 15 (black). The time distribution of the vaccines for  $N_{App} = 12$  is shown in Fig. 13(b). Figures 13(c) and 13(d) exhibit our results for 6073 available doses. The effect of vaccine application is less pronounced than in Fig. 10 due to the number of wasted doses to be larger, as shown in Fig. 13(b). The areas for these curves increase with the application number. Nevertheless, an increase in the application number implies an increase in the wasted doses. The effective doses decrease overtime, as a result of the increase in the number of exposed, infected and recovered cells overtime. Furthermore, we observe that in the scenario (iii), the number of effective doses in the application of consecutive groups decays exponentially according to  $\Delta t_v$ .

The difference between the scenarios with limited doses is that for the scenario (ii) the individuals are tested and then receive the vaccines, while in the scenario (iii), the vaccines are randomly distributed and consequently it is observed a larger waste of doses. In Fig. 14, the continuous lines show the results for the scenario (ii) and dash-dotted lines for the scenario (iii). These results demonstrate that the scenario (ii) is more effective than the scenario (iii) when the same number of doses are available.

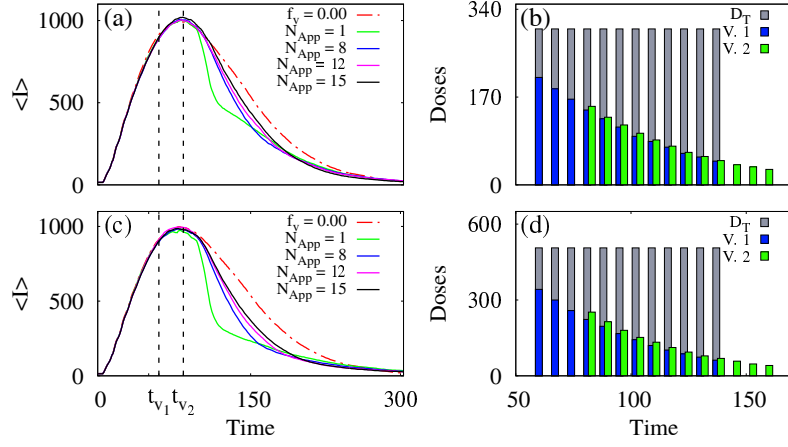


FIG. 13. (a) Average of infected curves overtime for  $N_T = 3621$  doses and  $N_{App}$  equal to 1 (green), 8 (blue), 12 (magenta), and 15 (black). (b) Time distribution of vaccines for  $N_{App} = 12$  with the effective vaccine for the first doses (blue bars), second doses (green bars), and available doses (gray bar). (c) Average of infected curves overtime for  $N_T = 6073$  doses. (d) Time distribution of vaccines for  $N_{App} = 12$  with the effective vaccine for the first doses (blue bars), second doses (green bars), and available doses (gray bar). The red dashed-dotted line is without vaccination. The black vertical dashed lines indicate the time of the first and second doses for the first cell groups. We consider  $\psi = 0.66$ ,  $\delta = 0.75$ , and  $\Delta t_v = 7$ . The time unit is day.

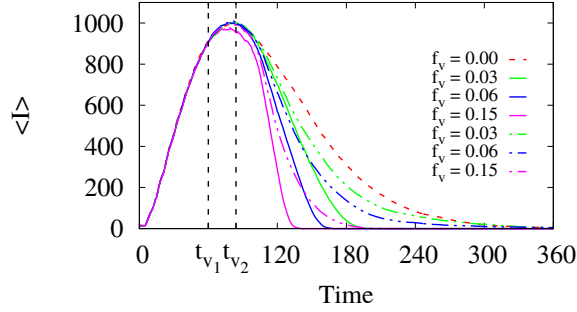


FIG. 14. Comparison between the scenarios (ii) (continued lines) and (iii) (dash-dotted lines). The vaccinations start at  $t_{v_1} = 60$  and  $t_{v_2} = 84$  (vertical dashed lines). The red dashed line is for the case without vaccination. We consider  $\psi = 0.66$ ,  $\delta = 0.75$ , and  $\Delta t_v = 7$ . The time unit is day.

Figure 15 displays the fraction of wasted dose as a function of  $N_{App}$  for the scenarios (ii) and (iii) by means of circles and squares, respectively. In some cases occur the waste in the first dose for the scenario (ii) due to the fact that the total quantity of available doses is larger than the number of susceptible individuals. In these cases, the average of wasted doses is equal to 0.01. In the second dose, the wasted doses in the scenario (ii) remains approximately constant, exhibiting an average value about 0.32. On the other hand, the wasted doses in the scenario (iii) have a linear dependency on the number of applications. For the first dose, the average of the wasted doses is about 0.60 and for second is about 0.72.

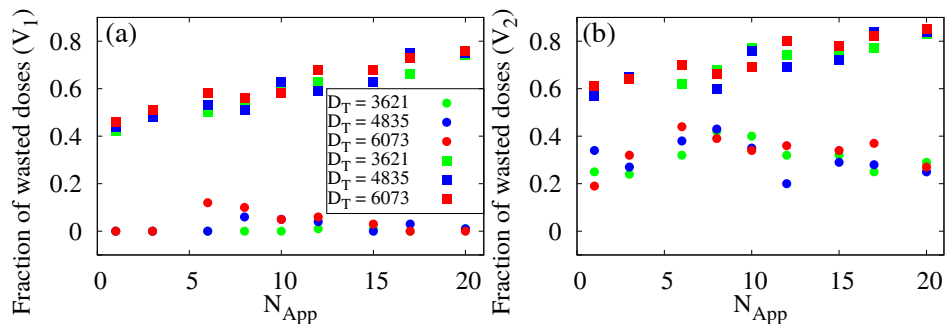


FIG. 15. Comparison between the fraction of wasted doses as a function of  $N_{\text{App}}$  in the scenarios (ii) (circles) and (iii) (squares) for the (a) first and (b) second doses. We consider  $\psi = 0.66$ ,  $\delta = 0.75$ ,  $\Delta t_v = 7$ ,  $t_{v_1} = 60$ , and  $t_{v_2} = 84$ . The time unit is day.

## V. CONCLUSIONS

In this paper, we introduce two vaccination doses in the SEIR model by means of a stochastic cellular automaton, named SEIR2V. We consider probabilistic transitions in our cellular automaton. There are transitions from susceptible to exposed states and from exposed to infected states after latent periods. The individuals in the infected state go to recovered states after an infectious period. In our model, the disease propagation occurs by contact in a two-dimensional space with a fix position, such as in a conduction process. A discussion of convection-like process, i.e. movements in the model, can be found in [46] and the influence in a CA model in [47]. In future works, we plan to analyse the effects of movement in our model. We use parameters that are related to types of illnesses and can be adapted for many other infectious diseases. Depending on the parameter values, it is possible to find an equilibrium point that is related to the disease-free.

In our model, we consider the inclusion of two new compartments, which are associated with the individuals vaccinated with the first and second doses. As a result, a fraction of individuals transit between these two states. The dynamic behaviour of the model depends on the time between the dose applications, the efficacy of the first and second doses, and the time of immunisation after the vaccine application. The inclusion of two doses vaccinations allows us to investigate the influence of different strategies to realised the immunisation of the individuals. In this work, we analyse two major scenarios, where there are unlimited and limited doses of vaccines.

Unlimited doses of vaccines are considered in the scenario (i), while limited doses are analysed in the scenarios (ii) and (iii). In the scenario (i), we observe that the cellular automaton converges early to a disease-free equilibrium for a fraction of individuals vaccinated with the first dose ( $f_v$ ) greater than 0.01 starting at a small time ( $t_{v_1}$ ). Similar results are found for other  $t_{v_1}$  values when  $f_v \geq 0.08$ . For small values of  $t_{v_1}$ , earlier eradicating points are achieved. More important than vaccine efficacy and delay between the first and second doses are the quantity of effective vaccination and how earlier the application starts.

The scenarios (ii) and (iii) are more realistic, since in real situations the number of doses is limited. The scenario (ii) represents the case in which all population is tested and only the susceptible individuals are vaccinated. In this scenario, we consider a new parameter  $\Delta t_v$ , which is the interval between the applications of vaccines in different groups. We verify that the vaccination is more effective for small intervals of applications. When the total available doses are divided into many applications, the best strategy is to administrate the doses through few applications. Despite the disease-free points, they are reached earlier when the number of applications ( $N_{\text{App}}$ ) is larger, while the total number of infected cells is small when  $N_{\text{App}}$  is small. In this strategy, the number of wasted doses in the first application is minimal ( $\leq 13\%$ ), while the fraction of wasted doses in the second application is in the range from 20% to 45%.

The scenario (iii) corresponds to the case in which the population is not tested and the available doses are randomly distributed. In this scenario, the vaccination is less effective than the scenario (ii) due to the number of wasted doses. The dose effectiveness decays exponentially according to  $\Delta t_v$ . The wasted doses can be minimised in this scenario by collecting the available doses and apply them just once. In this strategy, the number of wasted doses in the first and second applications exhibits approximately a linear growth with the number of applications, being larger than the scenario (ii).

All in all, independently from the strategy, the results can be improved when the vaccination campaign starts early and with a large number of vaccinated individuals.

## ACKNOWLEDGEMENTS

This work was possible by partial financial support from the following Brazilian government agencies: Fundação Araucária, CNPq (407543/2018-0, 302903/2018-6, 420699/2018-0, 407299/2018-1, 428388/2018-3, 311168/2020-5), CAPES (88887.485425/2020-00), and São Paulo Research Foundation (FAPESP 2018/03211-6, 2020/04624-2). We would like to thank 105 Group Science ([www.105groupscience.com](http://www.105groupscience.com)).

- 
- [1] S.L.T. de Souza, A.M. Batista, I.L. Caldas, K.C. Iarosz, J.D. Szezech Jr, Dynamics of epidemics: Impact of easing restrictions and control of infection spread. *Chaos, Solitons & Fractals* 142 (2021) 110431.
- [2] J. Dai, C. Zhai, J. Ai, J. Ma, J. Wang, W. Sun, Modeling the spread of epidemics based on cellular automata. *Processes* 9 (2021) 55.
- [3] S.H. White, A.M. del Rey, G.R. Sánchez, Modeling epidemics using cellular automata. *Applied Mathematics and Computation* 186 (2007) 193-202.
- [4] K.A. Glatzer, P. Finkelman, History of the Plague: An Ancient Pandemic for the Age of COVID-19, *The American Journal of Medicine* 134 (2021), 176-181.
- [5] T.M. Tumpey, C.F. Basler, P.V. Aguilar, H. Zeng, A. Solórzano, D.E. Swayne, N.J. Cox, J.M. Katz, J.K. Taubenberger, P. Palese, A. García-Sastre, Characterization of the reconstructed 1918 Spanish influenza pandemic virus. *Science* 310 (2005) 77-80.
- [6] A.M. Lauren, P. Babak, M.E.J. Newman, D.M. Skowronski, R.C. Brunham, Network theory and SARS: predicting outbreak diversity. *Journal of Theoretical Biology* 232 (2005) 71-81.
- [7] L. Mao, L. Bian, Spatial-temporal transmission of influenza and its health risks in an urbanized area. *Comput. Environ. Urban Syst.* 34 (2012) 204-215.
- [8] M. Voysey, S.A. Clemens, S. Madhi, L. Weckx, P. Folegatti, P. Aley, B. Angus, V. Baillie, S. Barnabas, Q. Bhorat, S. Bibi, C. Briner, P. Cicconi, E. Clutterbuck, A. Collins, C. Cutland, T. Darton, K. Dheda, C. Chritina, Single-dose administration and the influence of the timing of the booster dose on immunogenicity and efficacy of ChAdOx1 nCoV-19 (AZD1222) vaccine: a pooled analysis of four randomised trials. *The Lancet* 397 (2021) 881-891.
- [9] B.A. Mello, One-way pedestrian traffic is a means of reducing personal encounters in epidemics. *Frontiers in Physics* 8 (2020).
- [10] C. Balsa, I. Lopes, T. Guarda, J. Rufino, Computational simulation of the COVID-19 epidemic with the SEIR stochastic model. *Computational and Mathematical Organization Theory* (2021). <https://doi.org/10.1007/s10588-021-09327-y>
- [11] N. Sharma, A.K. Verma, A.K. Gupta, Spatial network based model forecasting transmission and control of COVID-19, *Physica A* 581(1) (2021), 126223.
- [12] X. Meng, Z. Cai, S. Si, D. Duan, Analysis of epidemic vaccination strategies on heterogeneous networks: Based on SEIR model and evolutionary game. *Applied Mathematics and Computation* 403 (2021) 126172.
- [13] V. Piccirillo, Nonlinear control of infection spread based on a deterministic SEIR model. *Chaos, Solitons & Fractals* 149 (2021) 111051.
- [14] M. Amaku, D.T. Covas, F.A.B. Coutinho, R.S.A. Neto, C. Struchiner, A. Wilder-Smith, E. Massad, Modelling the test, trace and quarantine strategy to control the COVID-19 epidemic in the state of São Paulo, Brazil. *Infectious Disease Modelling* 6 (2021) 46-55.
- [15] M. Amaku, D.T. Covas, F.A.B. Coutinho, R.S. Azevedo, E. Massad, Modelling the impact of delaying vaccination against SARS-CoV-2 assuming unlimited vaccine supply. *Theor. Biol. Med. Model* 18 (2021), 14.
- [16] A.M. Batista, S.L.T. de Souza, K.C. Iarosz, A.C.L. Almeida, J.D. Szezech Jr., E.C. Gabrick, M. Mugnaine, G.L. dos Santos, I.L. Caldas, Simulation of deterministic compartmental models for infectious diseases dynamics. *Rev. Bras. Ensino Fis.* 43 (2021).
- [17] A. Radulescu, C. Williams, K. Cavanagh, Management strategies in a SEIR model of COVID-19 community spread. *Scientific Reports* 10 (2020) 21256.
- [18] J.M. Carcione, J.E. Santos, C. Bagaini, J. Ba, A simulation of a COVID-19 epidemic based on a deterministic SEIR model. *Frontiers in Public Health* 8 (2020) 230.
- [19] L. Quan-Xing, J. Zhen, Cellular automata modelling of seirs, *Chinese Physics* 14 (2005) 1370.
- [20] E. Malkov, Simulation of coronavirus disease 2019 (COVID-19) sceneries with possibility of reinfection. *Chaos, Solitons & Fractals* 139 (2020) 110296.
- [21] P. Wintachai, K. Prathom, Stability of SEIR model related to efficiency of vaccines for COVID-19 situation. *Heliyon* 7 (2021) e06812.
- [22] M. Etxeberria-Etxaniz, S. Alonso-Quesada, M. De la Sen, On an SEIR epidemic model with vaccination of newborns and periodic impulsive vaccination with eventual on-line adapted vaccination strategies to the varying levels of the susceptible subpopulation. *Applied Sciences* 10 (2020) 8296.
- [23] M. Jadidi, S. Jamshidiha, I. Masroori, P. Moslemi, A. Mohammadi, V. Pourahmadi, A two-step vaccination technique to limite COVID-19 spread using mobile data. *Sustainable Cities and Society* 70 (2021) 102886.
- [24] M.A. Safi, A.B. Gumel, Mathematical analysis of a disease transmission model with quarantine, isolation and an imperfect vaccine. *Computers & Mathematics with Applications* 61 (2011) 3044-3070.

- [25] P. Yongzhen, L. Shuping, L. Changguo, S. Chen, The effect of constant and pulse vaccination on an SIR epidemic model with infectious period. *Applied Mathematical Modelling* 35 (2011) 3866-3878.
- [26] A. Nava, A. Papa, M. Rossi, D. Giuliano, Analytical and cellular automaton approach to a generalized SEIR model for infection spread in an open crowded space. *Physical Review Research* 2 (2020) 043379.
- [27] M. De la Sen, S. Alonso-Quesada, A. Ibeas, R. Nistal, On a discrete SEIR epidemic model with two-doses delayed feedback vaccination control on the Susceptible. *Vaccines* 9 (2021) 398.
- [28] M. Mugnaine, E.C. Gabrick, P.R. Protachevicz, K.C. Iarosz, S.L.T. de Souza, A.C.L. Almeida, A.M. Batista, I.L. Caldas, J.D. Szezech Jr, R.L. Viana, Control attenuation and temporary immunity in a cellular automata SEIR epidemic model. *Chaos, Solitons & Fractals* 155 (2022) 111784.
- [29] N. Sharma, A. K. Gupta, Impact of time delay on the dynamics of SEIR epidemic model using cellular automata. *Physica A* 471 (2017) 114-125.
- [30] M. Kotyrba, E. Volna, P. Bujok, Unconventional modelling of complex system via cellular automata and differential evolution. *Swarm and Evolutionary Computation* 25 (2015) 52-62.
- [31] S. Wolfram, *Cellular automata and complexity: collected papers*. 1. ed. Reading, MA: Addison-Wesley, 1994.
- [32] S. Wolfram, Statistical mechanics of cellular automata. *Reviews of Modern Physics* 55 (1983) 601.
- [33] S. Wolfram, *Cellular Automata*. Los Alamos Science (1983). URL: <https://content.wolfram.com/uploads/sites/34/2020/07/cellular-automata.pdf>
- [34] G. Schneckeneither, N. Popper, G. Zauner, F. Breitenecker, Modelling SIR-type epidemics by ODEs, PDEs, difference equations and cellular automata - A comparative study. *Simulation Modelling Practice and Theory* 16 (2008) 1014-1023.
- [35] F.S. Borges, E.L. Lameu, A.M. Batista, K.C. Iarosz, M.S. Baptista, R.L. Viana, Complementary action of chemical and electrical synapses to perception. *Physica A: Statistical Mechanics and its Applications* 430 (2015) 236-241.
- [36] F.S. Borges, P.R. Protachevicz, V. Santos, M.S. Santos, E.C. Gabrick, K.C. Iarosz, E.L. Lameu, M.S. Baptista, I.L. Caldas, A.M. Batista, Influence of inhibitory synapses on the criticality of excitable neuronal networks. *Indian Academy of Sciences Conference Series* 3 (2020).
- [37] S. Bin, G. Sun, C.C. Chen, Spread of infectious disease modeling and analysis of different factors on spread of infectious disease based on cellular automata. *International Journal of Environmental Research and Public Health* 16 (2019) 4683.
- [38] G.Y. Vichniac, Simulating physics with cellular automata. *Physica D* 10 (1984) 96-116.
- [39] L. Meacci, M. Primicerio, G.C. Buscaglia, Growth of tumours with stem cells: The effect of crowding and ageing of cells. *Physica A* 570 (2021) 125841.
- [40] R.L. Viana, F.S. Borges, K.C. Iarosz, A.M. Batista, S.R. Lopes, I.L. Caldas, Dynamic range in a neuron network with electrical and chemical synapses. *Communications in Nonlinear Science and Numerical Simulation* 19 (2014) 164-172.
- [41] L.B.L. Santos, M. C. Costa, S.T.R. Pinho, R.F.S. Andrade, F.R. Barreto, M.G. Teixeira, M.L. Barreto, Periodic forcing in a three-level cellular automata model for a vector-transmitted disease. *Physical Review E* 80 (2009) 016102.
- [42] V. Blavatska, Yu. Holovatch, Spreading processes in post-epidemic environments. *Physica A* 573 (2021) 125980.
- [43] A.R. Mikler, S. Venkatachalam, K. Abbas, Modeling infectious disease using global stochastic cellular automata. *Journal of Biological Systems* 13 (2005) 421-439.
- [44] A.L.B. Cavalcante, L.P. de Faria Borges, M.A. da Costa Lemos, M.M. Farias, H.S. Carvalho, Modelling the spread of covid-19 in the capital of Brazil using numerical solution and cellular automata. *Computational Biology and Chemistry* 94 (2021) 107554.
- [45] A. Ilachinski, *Cellular automata: a discrete universe*. World Scientific (2001). DOI: <https://doi.org/10.1142/4702>
- [46] V. Belik, T. Geisel, D. Brockmann, Natural human mobility patterns and spatial spread of infectious diseases. *Physical Review X* 1 (2011).
- [47] W.G. Weng, T. Chen, H.Y. Yuan, W.C. Fan, Cellular automaton simulation of pedestrian counter flow with different walk velocities. *Physical Review E* 74 (2006) 036102.